Rheo-PIV Analysis of the Yielding and Flow of Model Waxy Crude Oils

Christopher J. Dimitriou,[†] Gareth H. McKinley,[*,†] and Ramachandran Venkatesan[‡]

Department of Mechanical Engineering, Massachusetts Institute of Technology, Cambridge MA, and Chevron Energy Technology Company, Houston TX

E-mail: gareth@mit.edu

Abstract

Waxes are a commonly encountered precipitate that can result in gelation of crude oils and cessation of flow in pipelines. In this work we develop a model wax-oil system that exhibits rheological behavior similar to waxy crude oils encountered in production scenarios. To study the consequences of gelation on the rheology of the model system we perform simultaneous measurements of the bulk flow behavior using rheometry and of the local shearing deformation using Particle Image Velocimetry. The bulk rheological measurements are correlated to deviations from the linear velocity profile anticipated for a homogenous sample undergoing simple shear - this provides new insights into the structural and rheological evolution of these wax-oil systems under representative shearing conditions.

The restart of flow and breakdown of the gelled wax-oil structure is observed under two scenarios - a constant applied stress, and a constant applied strain rate. In addition, the effect of varying surface roughness on flow restart is investigated by comparing the temporal evolution

---

[*]To whom correspondence should be addressed
[†]Department of Mechanical Engineering, Massachusetts Institute of Technology, Cambridge MA
[‡]Chevron Energy Technology Company, Houston TX

of the velocity fields for an initially gelled fluid in contact with both a roughened and smooth surface. The material response in each case indicates that some classes of surface act as slip inhibitors and prevent the gelled wax-oil system from slipping against them. This promotes bulk deformation and the more rapid breakdown of the gel structure. These results are consistent with recent observations in other jammed/yielding systems and have an immediate bearing on pipeline restart strategies.

Introduction

Wax is a commonly occurring component of crude oil. It is generally characterized as consisting of large n-paraffins that are solid at room temperature when isolated, yet soluble in the crude oil mixture at elevated temperatures.[1] Waxy crude oils are crude oils with relatively high amounts of wax suspended in them.[2] The rheology of such materials is extremely sensitive to temperature, because at lowered temperatures it is possible for wax to precipitate out of the crude oil mixture and form a sample-spanning gel-like structure composed of crystallites with a high aspect ratio.[3] The sample spanning network formed by these crystallites is akin to a physical gel network in which the correlation length has diverged towards infinity,[4,5] and the high aspect ratio of the crystallites allows for gelation to occur at low volume fractions of precipitated wax.[6–8] Some studies have also suggested that the gel structure formed by the precipitates is a fractal network.[9]

There is considerable interest in developing an improved understanding of the rheology of waxy crude oils.[10,11] These particular types of crude oil are often encountered in deep water or ultra-deep water production scenarios where the temperature of the ambient sea water around tie-backs is particularly low.[6,12] Under such conditions, the tendency of waxy crude oils to form a percolated gel phase may result in the blocking of a flow-line that can cause a halt in production. After hydrate precipitates, wax precipitates are the second most common cause for blocked flow-lines in oil production scenarios.

In order to understand the yielding of these gel structures during a pipeline restart it is necessary to study the behavior of waxy crude oils at temperatures below the wax appearance temperature

(T_{wa}), which can be defined as the temperature at which wax precipitates first begin to form in the mixture. The formation of these precipitates affects the flow of the resulting multiphase system. Several approaches have been taken towards understanding the impact of wax precipitates on the rheology of these fluids and the practical applications thereof. Rheometric studies of waxy crude oils and waxy crude oil emulsions below their wax appearance temperature have been carried out by Visintin et. al.[13,14] The authors demonstrated that waxy crude oils exhibit a strongly temperature-dependent yield stress (σ_y) when they are below their wax appearance temperature. The yield stress represents the stress which must be exceeded in order for the oil to flow steadily and is important because it plays a critical role in determining the applied pressure drop required for restart of a gelled pipeline. Other workers have shown that thermal and shear history can have a significant effect on the strength of the gelled crude oil.[6,15–17] The nature of the "thermal beneficiation"[18] and cooling process used to form a gelled waxy crude oil thus plays an important role in determining the rheology of the gel. This beneficiation process typically involves heating the fluid to a temperature much higher than T_{wa} and shearing it for a designated amount of time. The fluid can then be cooled to below the gelation temperature at a prescribed cooling rate.

From data such as that presented by Visintin et. al., it is relatively straightforward to determine the yield stress of a gelled waxy crude oil. However, it is not clear how the value of a bulk yield stress σ_y determines the pressure required to restart a gelled pipeline. Recent work in the literature suggests that even model yield stress fluids can exhibit a complex transient yielding behavior. Gibaud and coauthors demonstrated (using localized velocity measurements) that Laponite suspensions exhibit rich temporal behavior as they undergo a yielding transition characterized by an initial shear localization period, followed by a period of "erosion" where solid fragments of the material break-down into smaller pieces.[19,20] Coussot et. al. have observed coexistence of liquid and solid regions in yield stress fluids under flow[21] and there has been additional work on connecting microstructural evolution of thixotropic yield stress fluids to their bulk rheology.[22,23]

For the restart of pipelines containing gelled waxy oil, complex spatial and temporal yielding behavior must be accounted for. Chang considered this type of yielding behavior by observing the

different stages of a flow restart in an isothermal pipeline.[24] However other factors may also affect restart behavior, for example, Perkins and Turner studied the restart behavior of gelled pipelines and determined that compressibility of the gel can play an important role in the restart procedure.[25] Furthermore, Lee et. al. have shown that it is possible for a gelled waxy crude oil to "break" or yield through either the mechanism of cohesive or adhesive failure.[26] These latter results suggest that when modeling the restart of a pipeline, the nature of the gel-wall interactions must be considered in detail as these can significantly affect the microstructure deformation processes that disrupt the gel.

The issue of determining a restart pressure from a simple measure of yield stress is also complicated by the fact that in most practical instances, the gel strength is not spatially uniform across the cross section of a pipe. This has been demonstrated by studying the process whereby wax precipitates deposit on pipeline walls and it has been shown that it is possible for waxes to deposit on the inner surface of a pipe if the temperature of the pipe wall is below the cloud point of the oil (or wax appearance temperature).[27] This incipient wax layer is the first step towards deposition of the gel on the pipe wall. The combined presence of spatial temperature gradients and diffusion of wax-forming molecules towards the cold wall has been shown to be responsible for the hardening, or 'aging' of the wax deposits closest to the pipeline wall.[28] In addition to this, non-uniformity in cooling rates across a pipeline can result in a spatially non-homogenous gel.

Due to the presence of a spatially heterogenous gel in a pipeline, it is typically difficult to develop predictions for restart behavior based on constitutive models for crude oil gels with a spatially uniform character. Despite this, there has been considerable effort expended in developing constitutive models to describe the rheology of waxy crude oils over a broad range of temperatures. Pedersen et. al. developed a Generalized Newtonian Fluid (GNF) model that describes the dependence of viscosity in a waxy oil on shear rate.[18] The authors used a modified Casson equation to describe this relationship - specifically the material parameters in the Casson equation were set to depend on the fraction of wax precipitated in the crude oil mixture. In recent efforts to improve quantitative agreement between experiments and theory, Ghanaei and Mowla showed good agree-

ment between experimental data and a model based on a combination of the Herschel-Bulkley model with the Richardson model.[29]

In the present work we connect bulk rheological behavior of the yielding transition in a model waxy crude oil with local measurements of deformation and wall slip effects. In order to understand what may affect the modes of yielding that occur in a waxy crude oil gel, we first outline the formulation of a model fluid developed to exhibit rheological characteristics similar to waxy crude oils. The Rheo-PIV system developed for flow assurance rheometry is then introduced and used to connect local velocity/deformation measurements to changes in the microscale structure of the gelled oil. The model fluid is used to observe the dynamical processes accompanying yielding behavior in a wax-oil gel and the changes induced by modifications of the wall boundary conditions. The structural evolution is studied through a combined approach of measuring the transient bulk rheological behavior while simultaneously observing spatial and temporal variations in localized velocity fields for a wax-oil gel under an imposed stress or strain rate. The observations of the local velocity fields within the wax/oil system under both imposed stresses and imposed shear rates show that roughened walls inhibit interfacial slip. Furthermore under a steady imposed shear rate, this inhibition of slip at the wall can result in a larger stress required to achieve steady flow and consequently more power being dissipated into the material. The larger rate of energy dissipation occurs alongside a much faster break down of the fluid structure - an observation that is verified through a metric based on the localized flow measurements.

Experimental Section

The Model Wax-Oil System

A model waxy oil was created that consisted of two components. The first (majority) component is a mineral oil used to form the continuous or matrix phase (Both a 'light' and 'heavy' version were used; Sigma Aldrich 330779 and 330760 respectively). The second component is a paraffin wax (Sigma Aldrich 327212) with a melting point specified by the manufacturer to be between 58°C

and 62°C. The composition of the light mineral oil and wax was examined through the use of Gas Chromatography, or GC. From the GC spectra, the wax was shown to contain a higher per-weight percentage of larger n-paraffins compared to the mineral oils. Furthermore, the wax contained only about 60%Wt. n-paraffins while the rest were iso- and cyclo-paraffins. The GC spectrum of the heavy mineral oil is similar to that of the light oil, with the weight percentage being generally higher at higher carbon numbers.

Thermorheological Behavior

The bulk thermorheological behavior of both the individual model fluid components, and the combined wax-oil system was studied using a TA Instruments AR-G2 stress controlled rheometer. A cone-plate geometry was utilized in order to ensure a uniform imposed strain field throughout the bulk of each sample and the upper and lower geometry surfaces were also roughened by using sandpaper with a root mean squared (rms) roughness $R_q = 30 \mu$m in order to avoid slip effects. Thermal control of the samples was achieved by using a lower plate equipped with a Peltier controller. The viscosity of the two mineral oils and the wax were measured as a function of their temperature (at a fixed shear stress, $\sigma = 2.8$Pa). The two mineral oils are Newtonian and exhibit increases in viscosity as temperature is decreased which can be modeled through the use of a simple Arrhenius equation,[30]

$$\eta = \eta_a e^{\frac{\Delta H}{R}\left(\frac{1}{T} - \frac{1}{T_0}\right)}, \tag{1}$$

Here η_a is the viscosity of the fluid at the temperature T_0, while ΔH is the activation energy for flow. Values of these parameters for the light oil are reported in Table 1 and the good agreement between the rheology of the model fit and the data is shown in Figure 1. Unlike the mineral oil, the paraffin wax shown in Figure 1 exhibits a much sharper increase in viscosity as it approaches its freezing temperature; it does not solidify immediately but rather exhibits a continuous (and large) change in viscosity over a drop in temperature of a few degrees. This arises from the formation of

6

the wax crystallites which consist of a range of n-paraffin components, each tending to crystallize at slightly different temperatures. As a result of this very localized transition from a Newtonian oil to a soft glassy solid-like material the thermorheological variations of the wax are modeled using a VFT (Vogel-Fulcher-Tammann) model,[31]

$$\eta = \eta_v e^{\frac{B}{T-T_\infty}}, \tag{2}$$

where η_v is the viscosity scale for the wax at very large temperatures, T_∞ is the temperature at which the viscosity of the wax diverges to infinity (which roughly corresponds to the melting temperature of the wax). The parameter B determines how fast the viscosity increases as the temperature of the wax is lowered. At very high temperatures, i.e. $T \gg T_\infty$, the VFT model approaches Arrhenius like behavior with the parameter equivalency $B = \frac{\Delta H}{R}$.
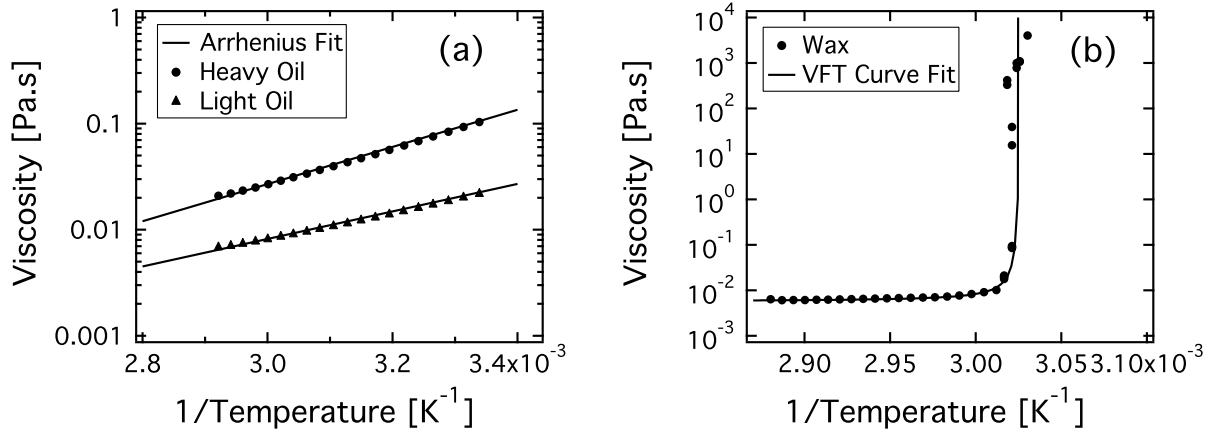

Figure 1: Temperature dependence of the viscosity for (a) the light and heavy mineral oil and (b) the paraffin wax. For the wax VFT fit, $B = 0.5$K, $T_\infty = 330.4$K and $\eta_v = 0.0056$ Pa.s. For the light oil $\eta_a = 0.0082$ Pa.s , $\frac{\Delta H}{R} = 2890$ K and for the heavy oil $\eta_a = 0.027$ Pa.s , $\frac{\Delta H}{R} = 3970$ K

The combined model wax-oil system consists of both the mineral oil and wax components (typically mineral oil with 5 or 10 wt.% wax). Thus, the model wax-oil system exhibits thermorheological behavior intermediate to the Arrhenius and VFT behavior of the oil and wax respectively. The dependence of viscosity on temperature for a range of wax-oil systems is shown in Figure 2. The viscosity of the wax-oil mixtures follows an Arrhenius like behavior for temperatures above

a certain value, and below this critical value their viscosity increases at a rate more rapidly than that predicted by the Arrhenius relation (but a slower rate than that predicted by the VFT equation for the pure wax). The temperature at which this marked change in behavior occurs is identified as the rheologically-relevant value of the wax appearance temperature, T_{wa}. By determining T_{wa} rheometrically rather than visually through turbidity data, we identify conditions at which wax precipitates first begin to dynamically impact the wax-oil system and lead to the super-Arrhenius behavior characteristic of a fragile liquid.[32] Values of T_{wa} for the range of model wax-oil systems shown in Figure 2 are given in Table 1.
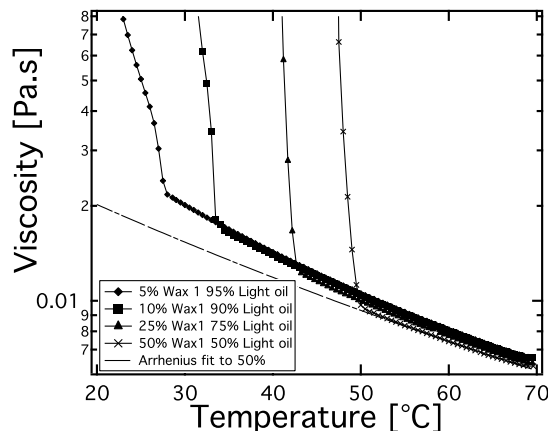

Figure 2: Temperature dependence of the steady shear viscosity at $\sigma_0 = 3$ Pa for several mixtures of wax in light oil containing different wt.% of wax. The broken straight line is an Arrhenius fit to the high temperature data for 50 wt.% wax at $T > T_{wa}$.

Table 1: Thermorheological parameters for various wax-in-light oil mixtures. For the Arrhenius fit in each case, T_0 is taken as 60°C.

	T_{wa} [K]	η_a [Pa.s]	$\frac{\Delta H}{R}$ [K]
Light Oil	N/A	0.0082	2890
5% Wax	302	0.0082	2877
10% Wax	306.5	0.0080	2845
25% Wax	316	0.0077	2717
50% Wax	324	0.0074	2443

The non-Newtonian rheological behavior exhibited by these fluids below T_{wa} is due to the formation of a percolated network of wax precipitates. It is possible to directly observe these

precipitates in the model wax-oil systems by placing a sample between crossed polarizers and illuminating the sample using monochromatic light under an optical microscope. Under these conditions, the structural anisotropy of the crystals gives rise to birefringence in the sample. Figure 3 shows an image taken using such a setup. The discotic wax precipitates can be seen as bright rod or needle-shaped objects due to being observed edge on in the 2 dimensional plane. The shape and size of these precipitates is consistent with observations reported previously in the literature for other wax-containing oils.[3,33]
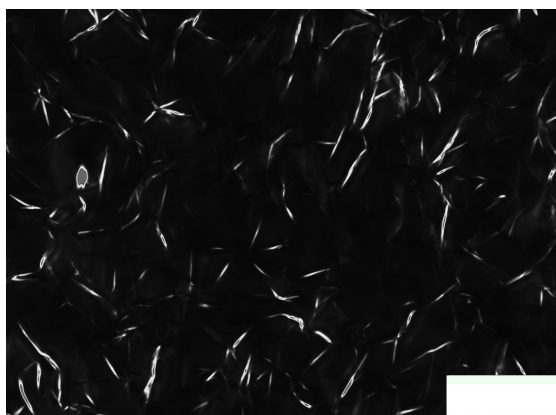

Figure 3: Birefringent microscope image showing the shape and size of wax crystallites formed in a 10% wax/light oil system under static conditions at 25°C ($T/T_{wa} = 0.987$). The scale bar on the bottom right has a length of 80μm.

Rheo-PIV System

In order to quantify the local yielding and deformation of the wax-oil system under an imposed shear rate or shear stress, a flow visualization system was constructed which allows for direct observation of the velocity field within a sample whilst undergoing shear in the rheometer. The principal goal of the Rheo-PIV system was to enable direct observation of yielding mechanisms in the model wax-oil system, such as those described by Lee.[26] The design of the system is similar to those implemented by Tapadia and Wang to study flow of entangled polymer melts[34,35] and Meeker et. al. for the study of soft pastes.[36,37] A schematic diagram for the setup is shown in Figure 4. A CCD camera is positioned orthogonally to the sample interface such that the imaging plane of the

lens/camera is located a few millimeters into the sample away from the fluid meniscus. The upper

(rotating) geometry of the rheometer is a 50mm diameter quartz plate, which allows illumination

of the sample using a collimated laser beam to form a focused imaging plane in the sample. The

laser is a focusable 10mW Edmund optics laser diode, with a wavelength of 635 nm. the sample

is seeded with reflective titanium dioxide seed particles from TSI Inc. of average size 3μm (much

smaller than the crystallites shown in Figure 3), allowing for the local velocity field across the

rheometer gap to be measured. The typical seeding density is 0.005%wt.. Figure 4 shows how

the lower shearing surface is attached to a raised Peltier configuration (TA instruments 531052)

and this allows several different bottom geometries to be used interchangeably, such as a cone

or a flat plate. For the tests involving the wax-oil mixture, precision-machined cones of radius

$R = 25$mm, angle $\Theta_0 = 4°$ and truncation 111 μm were used - the surface roughness of the cone

could also be modified by applying adhesive-backed sandpaper. Specifically, the solid surfaces

were either covered with an adhesive backed sandpaper with rms roughness, $R_q = 30\mu$m, or were

left uncovered having an rms roughness $R_q = 0.6\mu$m. The value of R_q was measured using a Zygo

interferometer. Specifically, for n measurements of the vertical distance of a surface from its mean

line (y_i), R_q is given by:

$$R_q = \sqrt{\frac{1}{n}\sum_{i=1}^{n} y_i^2} \tag{3}$$

The sequence of digital images obtained from the CCD camera is processed using a Particle

Image Velocimety (PIV) algorithm which applies a cross-correlation scheme to successive pairs

of images. This in turn provides a two-dimensional velocity vector field $\mathbf{v} = [v_x(x,y), v_y(x,y)]$

for each image pair obtained. By averaging the velocity vectors over the direction of flow (x-

direction) as well as over multiple images, it is possible to determine the average velocity pro-

file $\bar{\mathbf{v}} = [\bar{v}_x(y), \bar{v}_y(y)]$ across the gap of the rheometer. In order to demonstrate the accuracy of

the setup, Figure 5 shows a comparison of the measured velocity profile $\bar{v}_x(y)$ with the theoret-

ical profile expected for the low viscosity Newtonian mineral oil under a steady imposed shear

rate of $\dot{\gamma} = 0.535\text{s}^{-1}$. The control system of the rheometer imposes a steady shearing velocity
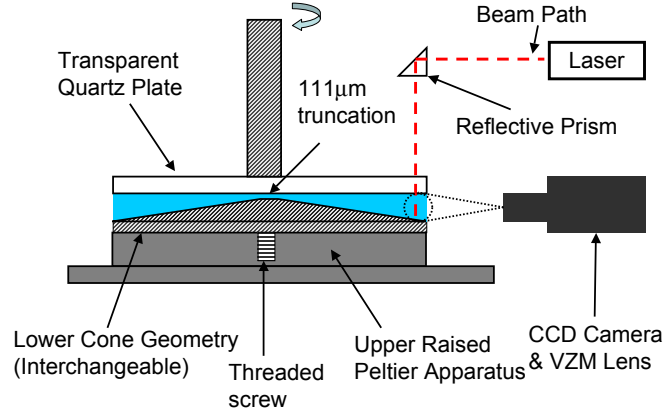
Figure 4: Schematic Diagram of Rheo-PIV System.

at the upper surface, and the magnitude of this velocity is shown at the top of the profile in Figure 5 and annotated as V_w. The theoretical shear rate and velocity profile are then specified to be $\bar{v}_x(y) = V_w \frac{y}{H} = \dot{\gamma}y$. As can be seen from Figure 5, the slope of the measured velocity profile is equal to the average shear rate within the gap and this agrees with the imposed shear rate that is set by the rheometer. The inset in Figure 5 gives the probability distribution of the velocity values over 180 frames and at the position $y = 0.7$mm from the lower plate (corresponding to $N = 4860$ observations). The distribution is Gaussian in nature, with a standard deviation, $\sigma = 0.0187$ mm/s, which is 5% of the mean value. The distribution of velocity measurements is similar at other positions within the gap and the standard deviation was found to vary between 0.014 and 0.023 mm/s. For the velocity in the vertical direction, $v_y(x, y)$, measurements give $\bar{v}_y = -0.011 \pm 0.04$mm/s.

Results and discussion

Bulk Yielding Phenomena

One defining characteristic of waxy crude oils is the existence of a yield stress below the wax appearance temperature.[13] As would be expected for a model system, the wax-oil mixture described
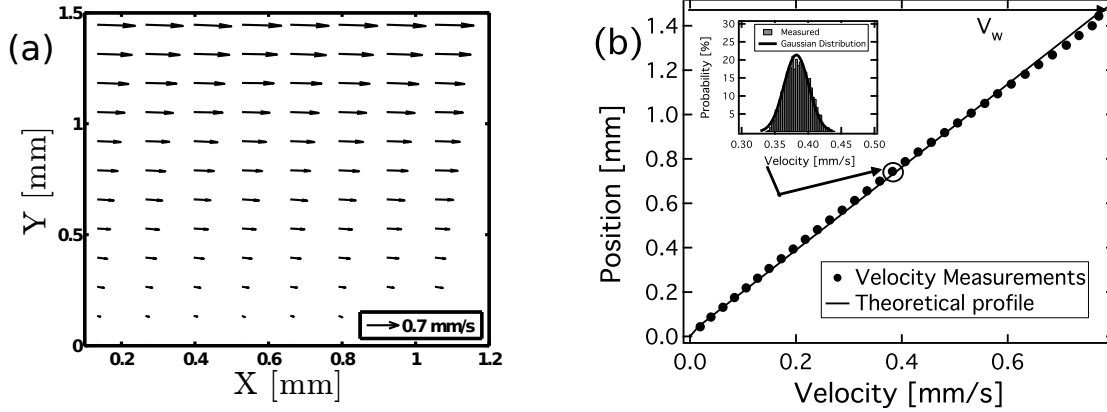
Figure 5: (a) 2D velocity field, and (b) averaged velocity profile, $\bar{v}_x$ of a 0.01% wt. seeded light mineral oil undergoing steady shear, $\dot{\gamma} = 0.535s^{-1}$. Inset shows the distribution of velocity vectors at a position $y = 0.7$ mm from the bottom plate.

above also exhibits a yield stress, with a magnitude that depends on temperature (shown in Figure 6). Experimental data from Visintin[13] demonstrated that the modulus of a crude oil gel (as parametrized by the viscoelastic moduli $G'(\omega)$ and $G''(\omega)$) below the wax appearance temperature can change depending on thermal history of the sample. Thus, to prevent any variability in the strength of the gelled system due to cooling rate differences, all systems were presheared at an elevated temperature $T = T_{wa} + 20°C$ for 10 minutes at a shear rate of 50 s^{-1} and then cooled at a rate of 1°C/min. A subsequent "holding time" of 10mins was then applied at the desired test temperature before each experiment. This particular sequence of steps is akin to the "thermal beneficiation" and cooling procedures described by Pedersen and is essential for obtaining repeatable measurements in these thermorheologically complex systems.[18] In addition to this, slip effects were avoided at the wall by carrying out the measurements using roughened upper and lower fixtures that ensure the no slip boundary condition is satisfied.

The data in Figure 6 shows the variation in the measured viscosity with applied shear stress, for the 5% wax-oil systems at a range of temperatures below $T_{wa} = 30.5°C$. In order to measure the very large (but finite) values of viscosity a creep test is carried out (in which a fixed stress is imposed) and the steady state viscosity is calculated 5 minutes after the imposition of stress from the measured rate of creep $\dot{\gamma} = \frac{d\gamma}{dt}$ and the imposed stress. It is apparent that there exists a
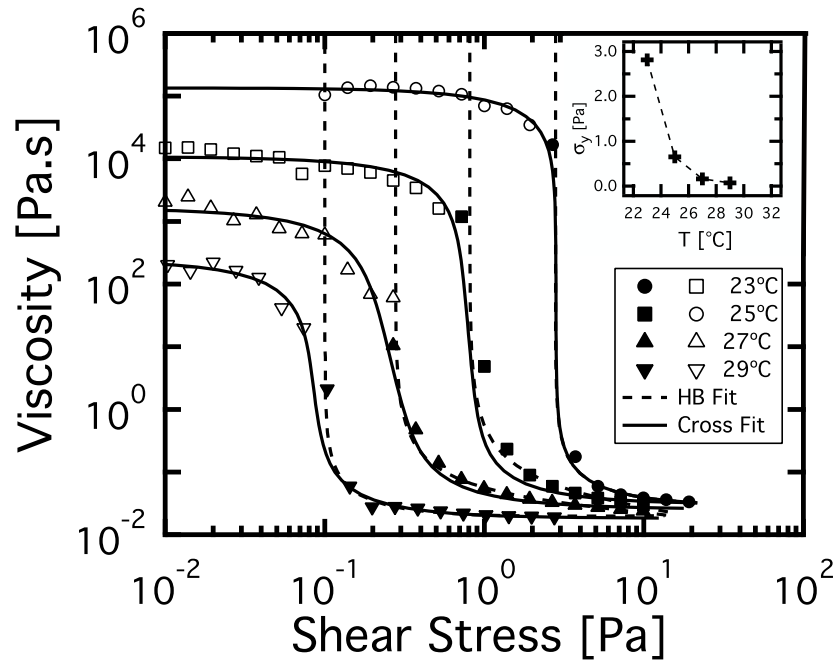
Figure 6: Flow curves for the 5% wax-light oil system at a range of temperatures below T_{wa}. Each set of points is fit to the Cross model for viscosity, which is given in equation Eq. (4), and the Herschel Bulkley (HB) model, given in Eq. (5). The hollow and filled symbols are used to distinguish the set of points used for the Cross fit (uses both hollow and filled) and the HB fit (uses only filled). The inset shows the variation of yield stress (σ_y based on the estimate from the Cross model) with temperature.

narrow range of stress values over which the viscosity of the fluid drops rapidly by several orders of magnitudes. This stress increases with decreasing temperature, and the drop in viscosity becomes more sudden at lower temperatures. Each data set is fitted to the Cross model:

$$\eta = \eta_\infty + \frac{\eta_0 - \eta_\infty}{1 + \left(\frac{\dot{\gamma}}{\dot{\gamma}^*}\right)^m} , \tag{4}$$

where η_0 and η_∞ are the limiting values of viscosity at low and high shear rates, respectively, the term $\dot{\gamma}^*$ is a critical shear rate associated with the sudden onset of shear thinning, and m is a parameter which controls the rate of thinning. The Cross model describes viscosity as a function of shear rate; however the data shown in Figure 6 is best represented with stress as the independent variable. Therefore, it is useful to understand that the critical stress or apparent yield stress predicted by the Cross Model is $\sigma_y \sim \eta_0 \dot{\gamma}^*$ (provided $\eta_0 \gg \eta_\infty$). The Cross model is successful at capturing simultaneously high and low shear stress behavior. Previous work has also utilized similar Generalized Newtonian fluid models in order to describe the flow behavior of waxy crude oils - specifically Visintin et. al.[13] used the RBC model (similar to the Cross model but with stress as the independent parameter instead of shear rate) to model yielding behavior of waxy crude with a finite low shear viscosity

Alternatively, if interest is limited to the flow curve beyond the point of yield, then the data in Figure 6 can also be fit to the Herschel-Bulkley model for high values of the stress (filled symbols corresponding to $\sigma > \sigma_y$):

$$\eta = \begin{cases} \frac{\sigma_{hb} + K\dot{\gamma}^n}{\dot{\gamma}} & \text{for } \sigma > \sigma_{hb} \\ \infty & \text{for } \sigma \leq \sigma_{hb} \end{cases} \tag{5}$$

The Herschel Bulkley model gives an independent estimate of the yield stress through the parameter σ_{hb}. This value can be compared with the estimate of σ_y obtained from the Cross model. The parameters used to fit each set of data in Figure 6 to the Cross model, as well as the resulting estimate of σ_y, are given in Table 2. For comparison, the value of the yield stress obtained from

14

the Herschel Bulkley model, σ_{hb}, is also provided in Table 2.

Previous work that has studied low shear rate viscosity plateaus in yield stress fluids has shown that the value of the low shear stress viscosity (η_0 for our case) may depend on measurement time.[38,39] For this reason, the value of η_0 that is determined from the Cross model fit is a lower bound on the zero shear rate viscosity because the measurement points were restricted to a time period of 5 minutes. However, the agreement of the values of σ_y and σ_{hb} to within a factor of 2 indicates that σ_y is still a physically relevant parameter - namely it is the critical stress value at which the material exhibits a very pronounced shear thinning behavior. The parameter σ_y is therefore similar to the "dynamic yield stress" which has been discussed by Chang et. al. as one of the measures for describing yielding behavior of waxy crude oils.[24,40]

Table 2: Parameters for the Cross model fit to model waxy crude oil data in Figure 6. Table includes value of yield stress parameter (σ_{hb}) for the Herschel Bulkley fitting.

	η_0 [Pa.s]	η_∞ [Pa.s]	$\dot{\gamma}^*$ [s^{-1}]	m [ ]	σ_y [Pa]	σ_{hb} [Pa]
23°C	1.35×10^5	2.80×10^{-2}	2.08×10^{-5}	1	2.81	2.80
25°C	1.08×10^4	3.06×10^{-2}	6.04×10^{-5}	0.97	0.6505	0.811
27°C	1.63×10^3	2.56×10^{-2}	9.80×10^{-5}	0.92	0.159	0.278
29°C	2.41×10^2	1.83×10^{-2}	3.04×10^{-4}	0.97	7.32×10^{-2}	0.103

The data shown in Figure 6 is representative of the bulk rheological behavior within the sample, and is not dependent on any type of interfacial slip interaction which might occur between the fluid and the solid surface of the cone-plate geometry. The no-slip boundary condition is ensured by using roughened upper and lower fixtures. Direct observations of the flow field using the Rheo-PIV system (as described above) show that this roughened geometry consistently prevents slip from occurring. Similar measurements can also be made with other yielding systems such as clay dispersions[19,20] and microgel pastes.[36,37]

Observations of the viscosity-stress dependence of the wax oil system after the fluid has been sheared to a considerable extent (and σ_y has been exceeded) have indicated that the yielding behavior exhibited by the fluid is an irreversible transition - i.e. the fluid does not recover its yield stress. The irreversibility inherent in the material can be demonstrated by measuring the viscosity of the

sample at incrementally higher values of shear stress (starting from stresses below the yield stress following the thermal beneficiation and cooling step). Eventually, when the yield stress $\sigma_y(T_{wa})$ is exceeded, the viscosity of the material drops drastically as the gel structure is disrupted. If the imposed shear stress is then lowered incrementally, the measured viscosity at stresses below the yield stress $\sigma < \sigma_y$ is observed to be lower by factors of 10-100 than it was in the pre-yielded state. This type of extreme time dependent behavior is illustrated in Figure 7; a 5% model wax in light oil system was beneficiated and cooled to 23°C at a rate of 1°C/minute and subsequently held for 10 minutes at 23°C. A series of creep steps was applied to the system, and the strain was measured over this period of time. The instantaneous viscosity of the sample is determined by computing the instantaneous strain rate $\dot{\gamma} = \Omega(t)R/\Theta_0$ at each point in time from the measured angular rotation rate $\Omega(t)$ of the fixture, and then dividing the applied stress by this instantaneous strain rate.

The sample initially creeps under an applied stress of 0.7 Pa for the first 15 minutes, followed by a creep step of 7 Pa for the next 15 minutes. Subsequently the stress is lowered again to 0.7 Pa for the next hour of the test. The stress of 0.7 Pa is below the yield stress of the 5% system at 23°C ($\sigma/\sigma_y = 0.26$). Thus, during the first 15 minutes of the experiment the system is in its pre-yielded state and creeps elastoplastically. When the larger 7 Pa stress is applied ($\sigma/\sigma_y = 2.6$), the percolated network of crystallites yields and the viscosity drops by a factor of 10^6 to a value of $\eta \sim 0.05$ Pa.s. During the third stress step at ($\sigma/\sigma_y = 0.26$), the viscosity recovers partially but it does not increase to the value initially exhibited in the pre-yielded state. Furthermore, even though the viscosity is measured over a period of 1 hour, it does not show any considerable increase over this period of time. Thus, the system does not show the distinctive rheological aging demonstrated in other yielding systems such as the Bentonite or Laponite suspensions studied by Møller and Coussot.[22,38,41] Similar behavior can also be demonstrated by other rheological tests such as "thixotropic loops".[38]

The irreversible yielding of an initially gelled wax-oil system can be understood by considering the forces which might drive a rearrangement of the wax microstructure. An analogy can be made between waxy crude oils and colloidal gels of anisotropic particles.[13] It is then possible to estimate
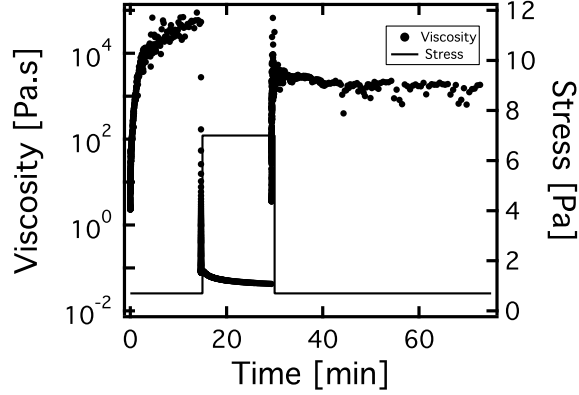
Figure 7: Irreversible yielding demonstrated by a viscosity vs. time plot for a 5% wax in light oil system at 23°C ($\sigma_y = 2.7$ Pa). in this particular experiment, 3 stress steps are imposed as indicated on the righthand ordinate axis: an initial step below the yield stress ($\sigma/\sigma_y = 0.26$), a second step above it ($\sigma/\sigma_y = 2.6$) and a third step again below the yield stress ($\sigma/\sigma_y = 0.26$). The sample does not restructure and the viscosity does not recover back to the pre-yielded value during the third step even over timescales of several hours.

the time scale required for Brownian forces to cause sufficient rotational diffusion of the wax crystallites to rearrange into a percolated network characteristic of the pre-yielded state. This time scale can be estimated using the following expression:[31]

$$\tau = \frac{a^3 \mu}{k_b T} \, ,$$ (6)

In Eq. (6), μ is the viscosity of the continuous phase (mineral oil $\eta_0 \sim 0.1$ Pa.s), T is the absolute temperature of the wax-oil gel, and a is the characteristic hydrodynamic size of the wax crystallites ($\sim 30\mu$m from Figure 3). From Eq. (6), we obtain a time scale of 7×10^5s, (i.e. on the order of weeks). Thus, in contrast to clay dispersions or colloidal gels, the wax microstructure is unable to re-establish the pre-yielded state through the action of Brownian motion alone and instead needs more complex rejuvenation strategies to ensure repeatable initial pre-yielded conditions (such as the thermal beneficiation and cooling procedure used in the present study).

17

Dependence of Material Response on Surface Conditions

As noted above, the rheological behavior described so far has assumed that the no slip boundary condition holds for the model wax-oil system under flow. This was ensured by using roughened upper and lower geometries (with roughness $R_q = 30\mu$m) for all rheological measurements. When the wax-oil system is placed in contact with smoother test fixtures the apparent bulk rheological behavior changes drastically due to the presence of slip.
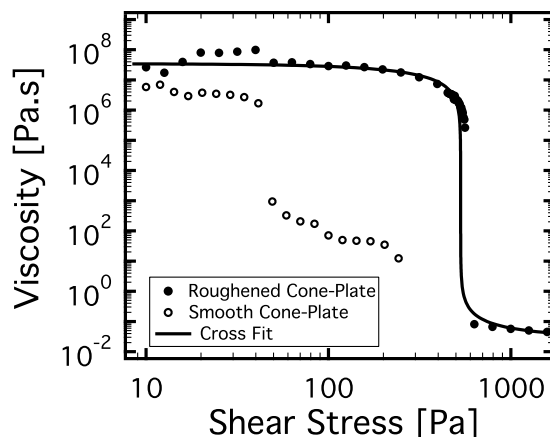

Figure 8: Viscosity-stress curve for a 10% wax in light oil system at 23°C ($T/T_{wa} = 0.980$) measured using a cone and plate geometry with roughened surfaces ($R_q = 30\mu$m) and a cone and plate geometry with smooth surfaces ($R_q = 0.6\mu$m).

One artifact of this slip presents itself in plots of the apparent viscosity for a 10% model wax-oil system experiencing steady shearing against each surface as shown in Figure 8. At high stresses, i.e. $\sigma \gtrsim 300$Pa, steady state can not be attained with the smooth surface under imposed stress conditions due to the instrument exceeding its maximum shear rate. However the data in the two cases can still be compared for lower stresses, i.e. values of $\sigma < \sigma_y$. For these values of stress the measured viscosity for the sample in contact with the smooth geometry is much lower than expected. A decrease in the apparent viscosity for values of $\sigma < \sigma_y$ is also observed for the 5% system, however this effect is less pronounced due to the weaker gel structure in the 5% system.

Barnes[42] shows a similar type of behavior for a printing ink, explaining that the lower viscosity in the case of the smooth surfaces is the result of slip at the fluid-solid boundary. In order to show that the discrepancy between the data in Figure 8 is a result of interfacial slip, the Rheo-PIV system

18

is used in conjunction with lower cone surfaces of different roughness. Specifically, a sequence of creep tests was carried out on a wax-oil system cooled to below T_{wa}, in which the imposed stress is incrementally stepped (in a logarithmic fashion) from a value below the yield stress to a value above it. For each of the creep steps, the imposed stress is held for a period of 60s, the macroscopic strain is recorded and a video recording (at 18 frames per second) was acquired for later PIV analysis to determine the local flow field within the sample. This sequence of creep tests was carried out for the wax-oil system in contact with a roughened lower geometry (again achieved using adhesive backed sandpaper), and for a smooth lower geometry. In both cases (and all other cases where the Rheo-PIV system is used to measure the velocity field) the upper geometry was a smooth quartz glass plate ($R_q = 0.02\mu$m), which is necessary to allow a path for the laser beam. In this experiment, a 5% wax-oil model fluid was used at a higher test temperature (27°C ; $T/T_{wa} = 0.993$), such that turbidity induced by the crystallites was still small. The conditions of this experiment differ from those of Figure 8 in several ways. Specifically, a lower wax content system is used at a higher temperature, and roughness on only the bottom surface is varied, while the upper surface is kept smooth. However, changes in the apparent strain with roughness can still be compared with the localized velocity measurements - these comparisons will show whether or not the changes are a result of varying degrees of slip occurring on the lower surface.

The bulk rheological data from this particular experiment is shown in Figure 9 in the form of the torsional strain $\gamma(t)$ response measured at each imposed stress σ_0. It is apparent that the waxy oil exhibits much larger straining displacements and larger strain rates when it is in contact with a smooth lower surface. Hence, the apparent viscosity computed by the rheometer using the definition $\eta \equiv \sigma_0/\dot{\gamma}(t)$ is generally lower. This behavior is consistent with the bulk rheological data shown in Figure 8. The important role of interfacial slip can be quantified through the analysis of the corresponding time-resolved PIV data corresponding to the creep tests in Figure 9. For each step in stress applied, the time period over which the material experiences substantial deformation is studied, such that it is possible to register a large enough displacement of the seed particles using the imaging system (typically a displacement of ≥ 1 pixel between frames is required). For the
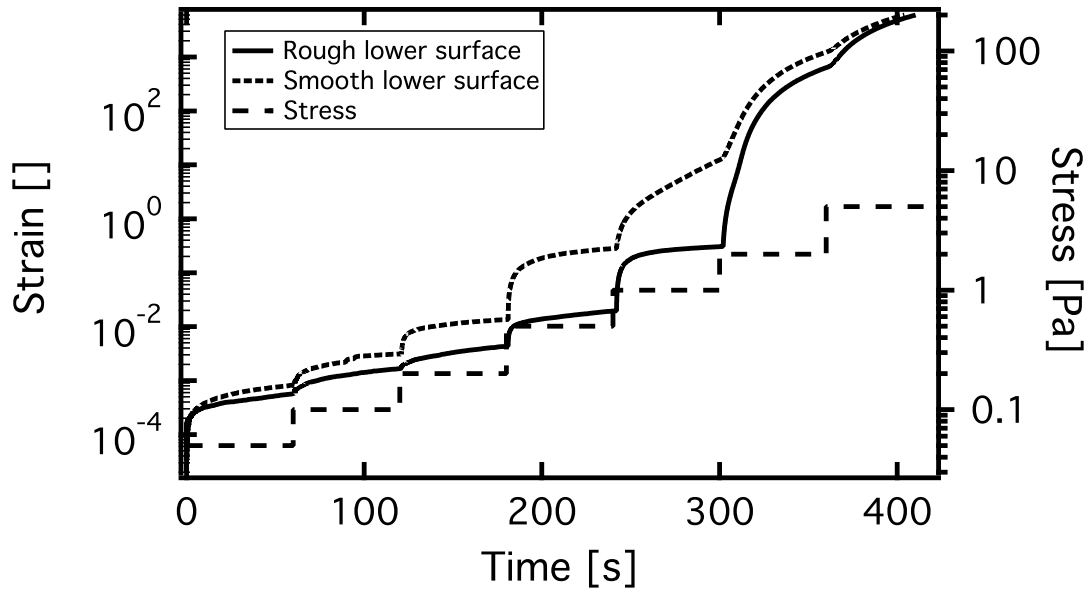
Figure 9: Sequence of creep tests used to restart flow of the 5% wax in light oil system.

sample in contact with the smooth lower fixture, this time period occurs beginning at the 240s mark, when the imposed stress is $\sigma = 1$ Pa. On the other hand, for the roughened case the velocimetry system only registers a displacement large enough when the imposed stress reaches $\sigma = 2$ Pa. Representative velocity profiles are shown on the left in Figure 10 for the wax-oil system during each of these steps. These velocity profiles show that the mechanism through which the material yields is markedly different in both cases. In the case of the roughened lower surface, the no slip condition is enforced at the lower plate, and flow occurs primarily through the mechanism of a non-zero shear rate in the bulk and a large slip velocity at the upper (smooth) surface. The instantaneous wall velocity $V_w = \Omega(t)R$ for each profile is indicated in the legend.

The full velocity profiles at these three instants in time after the imposition of the stress $\sigma_0 = 2$ Pa are shown to the left in Fig 10 (a) - these profiles show a positive, time-increasing average shear rate within the bulk in addition to pronounced slip. Furthermore, spatial variations in the shear rate $\dot{\gamma}(y)$ indicate that the material is experiencing higher shear rates near the upper surface. Distinctly shear-banded profiles (i.e. profiles with a discontinuity in shear rate, such as those observed in other yielding systems[43,44]) are not apparent, however the shear rate does show considerable spatial variations across the gap. Specifically, for the velocity profile at $t = 308.5$s, the shear rate varies

20

by a factor of 3 across the gap.

When the no slip boundary condition is relaxed on the lower plate (by using a smoother surface) the velocity profile appears to be plug-like. This is characterized by large slip velocities at the upper and lower surfaces ($v_s = 0.15$mm/s at the lower surface and $v_s = 0.05$mm/s at the upper surface) as well as a low average shear rate within the bulk ($\dot{\gamma}_{\text{bulk}} \simeq 0\text{s}^{-1}$). The critical role of wall roughness in mediating the importance of interfacial slip is not surprising for this model system, and similar effects have been observed in a wide variety of systems, including emulsions,[45] microgels,[23] pastes[36,46] and micellar fluids.[47]
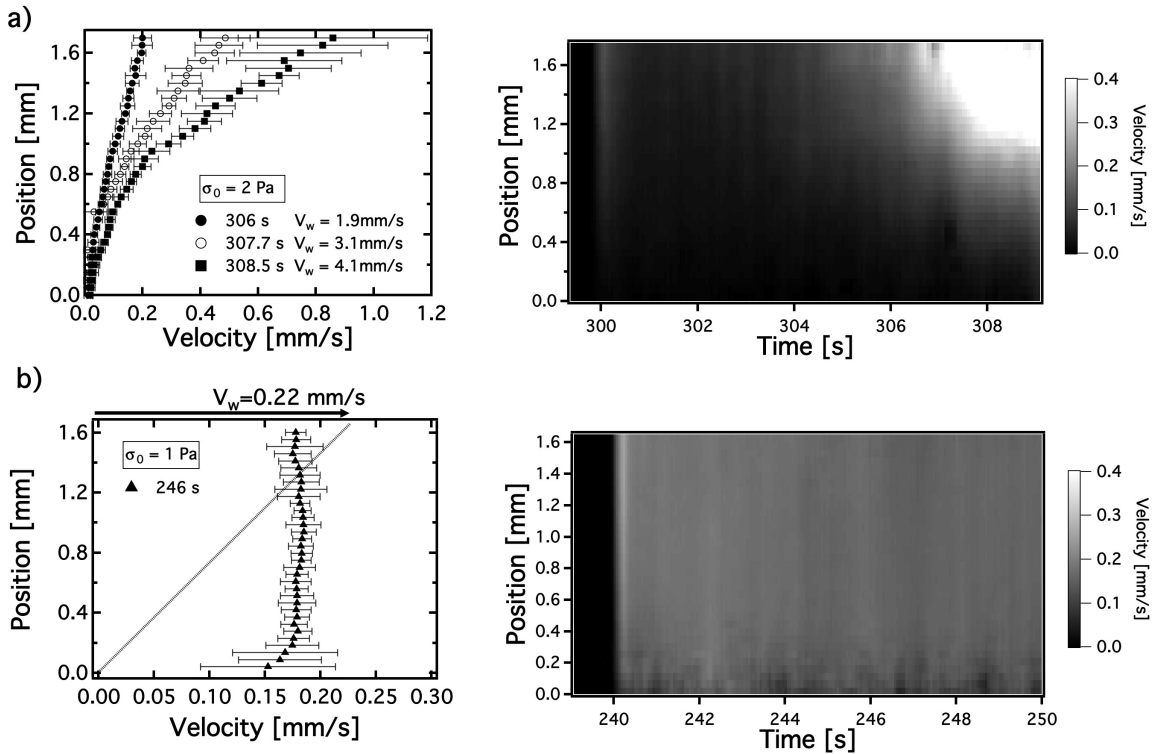

Figure 10: The space time diagrams $v_x(y,t)$ indicating evolution of the velocity profile within the wax-oil system for creep tests shown in Figure 9. In (a) the lower fixture surface is roughened ($R_q = 30\mu$m), in (b) the lower surface fixture is smooth ($R_q = 0.6\mu$m). Three representative instantaneous velocity profiles are shown on the left at $t = 306, 307.7, 308.5$ s for (a) and $t = 246$s for (b). The upper wall velocity, $V_w(t)$ is also shown in the legend for each profile.

The velocity profiles presented in Figure 10 are averaged over one frame of video, however the total number of frames for each creep test totals over 1000. As a result, it is possible to use a larger sequence of frames to determine the velocity profile within the gap over a larger period

of the creep test. In order to illustrate the evolution of the velocity field compactly, the profiles are represented in the form of a space-time diagram. These diagrams allow one to easily discern the evolution of the velocity profile within the rheometer gap over a long period of time, and have been used previously in the literature to understand time-evolving velocity fields.[19,48] For a space time diagram of steady homogenous shear flow with $v_x(y,t) = \dot{\gamma}y$, the diagram should appear as a uniform gradient vertically. Figure 10 shows spatiotemporal diagrams for the roughened creep test beginning at 300 s ($\sigma_0 = 2$ Pa), and the smooth creep test beginning at 240 s ($\sigma_0 = 1$ Pa).

The spatiotemporal diagrams reinforce the slip phenomena indicated by the instantaneous velocity profiles in Figure 10. The smooth lower surface allows for substantial slip to occur, resulting in an apparent flow of the material at a lower stress. Due to the occurrence of slip on the upper and lower surfaces the velocity field within the bulk of the wax-oil is uniform plug-like and accompanied by slip at both surfaces.

The data in Figure 10 verify that the wax-oil system can flow at lower shear stresses through the mechanism of slip on the solid surface. However, this behavior does not preclude bulk yielding at higher shear stresses. In fact, when the velocimetric data from the 2 Pa creep step (beginning at 300 s) for the smooth surface case is analyzed (data not shown), the shear rate within the bulk of the sample grows to be non zero. Interfacial slip still occurs, however the flow of the material is due to a combined effect of both wall slip and shearing in the bulk. Eventually, at high enough shear stresses ($\sigma_0 \geq 5$Pa), the creep curves shown in Figure 10 for the two different test configurations converge, indicating that at high shear stresses the contribution of slip to the total deformation is negligible, and the microstructure in the bulk material has broken down enough in both instances such that they are able to deform homogeneously throughout the gap. At these high shear stresses, surface characteristics have no effect on the flow. The viscosity value which is measured at these high stresses is approximately $\eta_{app} = 0.04$ Pa.s, which is consistent with values measured directly in steady shear flow for the 5% wax-oil system at a temperature of 27°C ($T/T_{wa} = 0.993$) with $\sigma \gg \sigma_y$ in Figure 6.

Figure 10 illustrates the time varying behavior of the velocity field within the material under a

constant stress. Instead of imposing a constant stress on the material, it is also possible to impose a constant strain rate on the material and simultaneously observe the velocity field within the sample. Constant shear rate experiments are a more common methodology used in probing crude oil rheology, and many constitutive models are fitted to experimental data from steady shear rate tests.[18,29] Under such conditions, one can discern whether or not velocity profiles such as the ones shown in Figure 10 are stable over a longer period of time. To probe the constant shear rate rheology, the 5% wax-oil system was cooled to a temperature of 27°C, and after beneficiation and cooling an imposed shear rate of $\dot{\gamma} = 0.3\text{s}^{-1}$ was applied to the material for a period of 10 minutes (in this test the smooth cone-and-plate geometry was used). The evolution in the bulk stress $\sigma(t)$ in the material was measured during this 10 minute period, as well as the local velocity field $\mathbf{v} = [v_x(x,y), v_y(x,y)]$ within the sample. The lefthand plot in Figure 11 shows the bulk stress in the material calculated by the rheometer following start up of steady shear flow; the stress passes through a peak value after approximately 20 seconds. It subsequently relaxes monotonically toward a lower equilibrium value ($\sigma \simeq 0.35$ Pa). The bulk averaged rheological behavior appears smooth, however the space-time plot in Figure 11 shows the time varying behavior of the local velocity field in the sample which fluctuates considerably over the course of the 10 minute test period.

At the bottom of Figure 11, velocity profiles at three different points in time are plotted in order illustrate the three different stages of flow exhibited by the wax-oil gel. The first profile is measured at the $t = 1\text{s}$ mark on the time axis of the space time plot in Figure 11 (this corresponds to 1 second after the shear rate of 0.3s^{-1} is imposed). The velocity profile at $t_1 = 1\text{s}$ is clearly linear - indicating that the material is exhibiting a uniform strain rate within its bulk, albeit with substantial slip occurring on the top surface. The second profile is measured at the 20 second mark. At this point, the profile appears to be almost perfectly plug-like. There is essentially zero strain rate within the bulk, with a slip velocity at both the top and bottom surfaces (these slip velocities are roughly equal, with a relationship between the slip velocity v_s and upper wall velocity v_w of $v_s \simeq v_w/2$). This plug-like profile is not stable in time, because the third velocity profile (which is
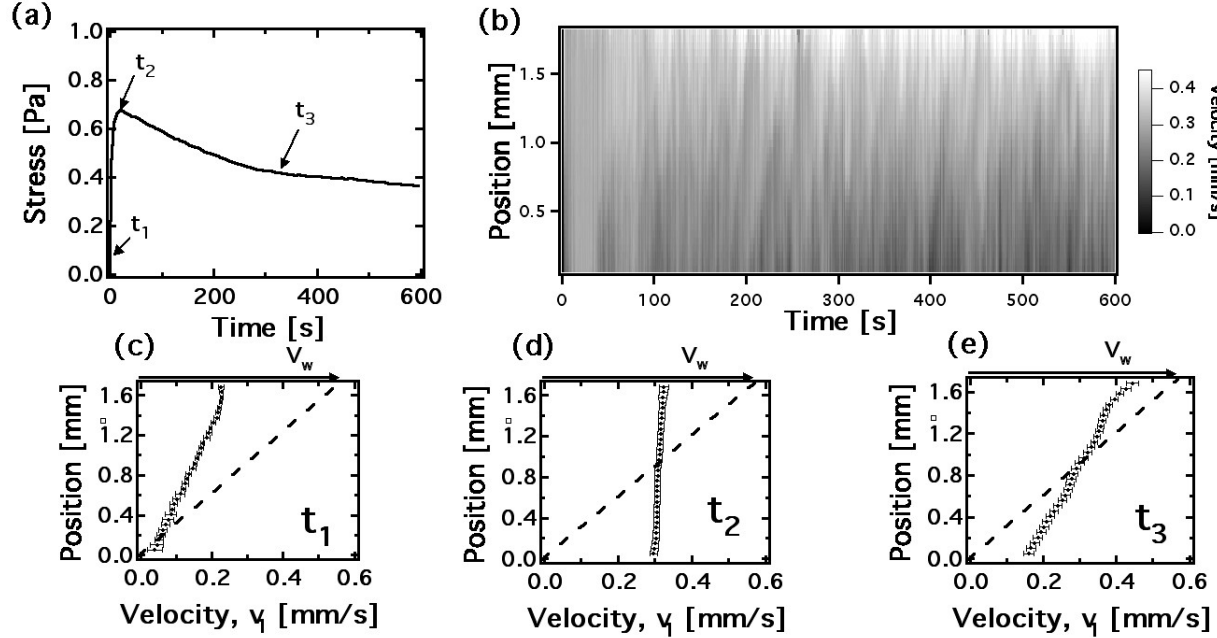
Figure 11: Bulk rheology (a) and local velocity field (b) for the 5% wax in light oil system undergoing a shear rate of $0.3\mathrm{s}^{-1}$ at 27°C ($T/T_{wa} = 0.993$). The velocity profiles at the bottom, starting from the left are at (c) $t_1 = 1$s; (d) $t_2 = 20$s; (e) $t_3 = 300$ s.

plotted at $t_3 = 300$s) shows that the material exhibits a non-zero shear rate within its bulk. However there is still slip occurring at the upper and lower surfaces. These slip velocities are roughly equal, so it is simple to calculate the true shear rate (averaged across the gap) experienced by the fluid from the Mooney expression:[49]

$$\dot{\gamma}_{\mathrm{true}} = \dot{\gamma}_{\mathrm{app}} \left(1 - \frac{2v_s}{v_w}\right), \tag{7}$$

Applying this formula to the profile at the 300 second mark, the value of the true shear rate is $\dot{\gamma}_{\mathrm{true}} = 0.17\mathrm{s}^{-1}$.

Both the slip velocity and the shear rate within the bulk fluctuate continuously over the duration of the experiment and these fluctuations are highlighted in the space time plot. As a result of these fluctuations, the transition from the second to the third stage of flow is neither fast nor smooth - there are periods of time when the shear rate within the bulk, and the slip velocity, rapidly vary. These stick-slip fluctuations indicate that the material is spatially heterogenous in the flow direc-

24

tion, consisting of localized regions in the bulk which are fluid-like and experience higher shear rates, and other regions where the sample is locally rigid and experiences little or no deformation. Furthermore, despite the lack of distinctly banded velocity profiles that have often been observed in some other systems,[34,43,44] there is still clearly heterogeneity of the material across the gap. This is illustrated by the variations in the shear rate $\dot{\gamma}(y)$ with the position (shown in Figure 11 (e)). To explore the heterogenous structuring in further detail we use a microscope-based optical imaging and shearing apparatus (Linkam CSS450 Shear Cell) consisting of two parallel, concentric, transparent plates between which a fluid sample is placed. One of the plates is connected to a motor and imposes a torsional deformation identical to what it would experience in a parallel plate rheometer. The Linkam shear cell allows for optical access through the plates, such that the local fluid microstructure can be imaged using a high magnification microscope objective.
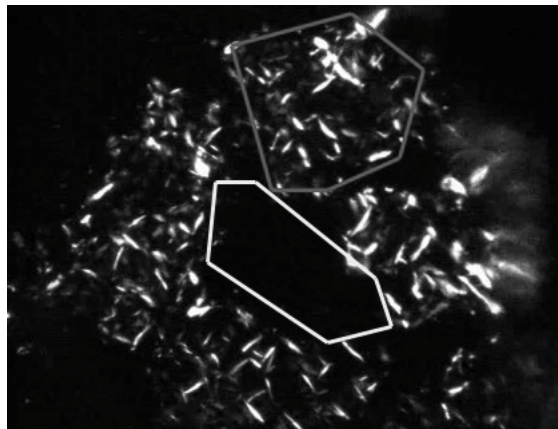

Figure 12: 10% wax in light oil system experiencing steady shear of $\dot{\gamma} \sim 0.1 \mathrm{s}^{-1}$ at temperature of 25°C ($T/T_{wa} = 0.964$) in the Linkam cell. To image the fluid an Edmund Optics Techspec VZM 600i lens was used in conjunction with a CCD camera. Vertical image size is roughly 1 millimeter. See supporting information for movie.

By placing the Linkam cell between crossed polarizers, the mesoscale structure and movement of individual wax precipitates can be observed more clearly under flow than using the Rheo-PIV system. However, instead of observing the deformation of the fluid in the 1-2 (flow-gradient) plane the Linkam acquires images in the 1-3 (flow-vorticity) plane.

In Figure 12 we show an image of a 10% wax-oil system experiencing steady shear in the Linkam cell at a shear rate of $\dot{\gamma} = 0.1 \mathrm{s}^{-1}$ and identify two specific regions of the image encircled

25

by bounding boxes. The region encircled by the lighter box is dark with no birefringence, and thus contains no precipitates within it; in this region the wax/oil mixture behaves as a Newtonian fluid. On the other hand the other region is a solid fragment (consisting of multiple wax crystallites) which flows essentially as a rigid body i.e. it does not deform over time (but it does translate linearly and rotate). The arrangement of these crystallite fragments is random, however under steady shearing they progressively break down and the average size decreases with time. During a pipeline restart operation one would thus expect local domains characteristic of plug-like flow profiles (resulting from the large fragments) to decrease over time as the stresses which cause the shearing deformation in the material steadily reduce the size of the fragments. This is consistent with the observations for the 5% wax-oil system under a steady apparent shear rate (Figure 11). Specifically, an initial plug-like flow profile is observed at the 20 second mark, however at the 600 second mark the flow observed more closely resembles a linear profile (with some wall slip still present however).

The process whereby these solid fragments break down is analogous to "shear melting" which has been observed in other yielding systems[50] and can be thought of as a transition from a jammed to an unjammed state within a phase diagram.[51] More specifically, the behavior observed in the model wax-oil system is similar to the process of fragmentation and erosion that Gibaud and coauthors describe in their work on another yielding fluid (a Laponite suspension).[20] Gibaud et. al. utilized a dimensionless metric based on frequency of observed plug like velocity profiles to quantify how much erosion had been experienced by an initially gelled fluid. Motivated by this analysis, a dimensionless measure Φ was developed in order to quantify the degree of erosion in the wax-oil mixture under a steady shear rate. This metric is shown schematically in Figure 13 and corresponds to a dimensionless and normalized measure of the area between the actual measured velocity $v_x(y)$ at each time t and an ideal linear velocity profile ($v_x = \dot{\gamma}y$). This measure can be evaluated from the following integral:

$$\Phi = \frac{1}{\dot{\gamma}H^2/4} \int_0^H |(v_x(y) - \dot{\gamma}y) - (\bar{v}_x - \dot{\gamma}H/2)| dy \tag{8}$$

where the first term in brackets in the integrand represents the difference between the local velocity $v_x(y)$ and the expected viscometric value $\dot{\gamma}y$, while the second term represents the difference between the average measured velocity and the average velocity for viscometric flow on the centerline at $y = H/2$. For any velocity profile Φ will vary between 0 and 1. These two limits correspond to the case of the linear velocity profile expected in Couette flow ($\Phi = 0$ and $v_x(y) = \dot{\gamma}y$, as shown in subfigure (a) in Figure 13) and the case of a plug like flow profile ($\Phi = 1$ and $v_x(y) = V_p$ where V_p is the velocity of the plug, as shown in subfigure (c) in Figure 13). When $\Phi \simeq 1$ and the fluid is experiencing plug like flow, the wax-oil gel consists of one fragment, or a few very large fragments, that slip along the top and bottom surfaces. A value of Φ approaching zero indicates that the gelled fragments have broken up and become smaller. Although Φ cannot provide a measure of the size of gel fragments, changes in its value do correspond to higher or lower degrees of fragmentation, and thus indicate whether or not the gel fragments have decreased or increased in size over time.
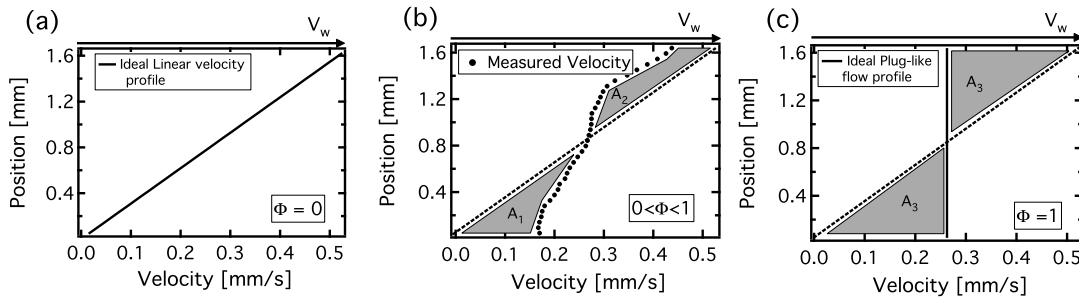

Figure 13: Schematic diagram indicating the parameter Φ. For the velocity profile (b) in the middle figure, Φ is given by $\frac{A1+A2}{2(A3)}$.

The computed evolution of $\Phi(t)$ for the data in Figure 11 is shown in Figure 14. There are large local fluctuations over short time intervals; however, the long term decay of $\Phi(t)$ is evidence of the progressive erosion of the structure and reflects the role of applied deformation on the increasing structural homogeneity of the wax-oil sample. We also note that there is an initial time period ($0 \leq t \leq 20$s) where Φ increases from zero to a maximum. This occurs due to the fact that the sample initially experiences a uniform elastic straining within the bulk and then slips to develop a plug like flow profile after 20 seconds. The point at which Φ reaches a maximum and the plug

27

like flow profile is established corresponds to the time t_2 in Figure 11 and coincides with passing

through a local maximum in the measured stress acting on the sample. At t_2, the maximum strain

has been accumulated in the fluid and from thereon flow occurs through a combination of wall slip

and a local fracturing behavior as indicated by the decreasing value of Φ. During this period the

applied stress on the material decreases (as shown in Figure 11) as the microstructure is progres-

sively eroded. The short term fluctuations in $\Phi(t)$ can be attributed to the spatial heterogeneity

of the sample. The Rheo-PIV imaging system only observes a small portion of the entire sample

(corresponding to 1mm field of view along the circumference). From the known circumference of

the fixture (~ 160mm) and the imposed rotation rate it is straightforward to calculate that it takes

300 seconds to make one full revolution at an imposed shear rate of 0.3s^{-1}. This time period is
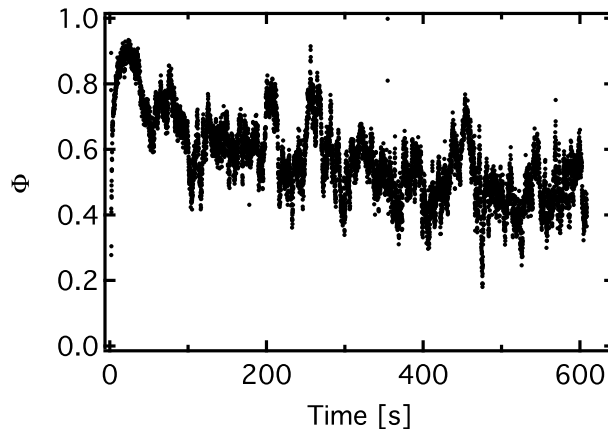
half of the duration of the entire experiment.

Figure 14: Evolution in the flow heterogeneity and erosion in the structure under steady shearing for the space-time data given in Figure 11 ($\dot{\gamma} = 0.3\text{s}^{-1}$ and $T/T_{wa} = 0.993$).

In order to observe the long term behavior of the fluid (and illustrate the steady state reached

by the system under steady shearing conditions), data for the parameter Φ is shown in Figure 15

for the same system as in Figure 14 (5% wax/oil mixture at 27°C) undergoing a larger steady shear

rate ($\dot{\gamma} = 1.5\text{s}^{-1}$) for a longer period of time (1600 s). For this case, the same surface conditions are

used as in in Figure 14. Figure 15 presents a locally averaged value of Φ over 0.5 second intervals

(31 frames per interval) at each data point. The result of this temporal averaging is to smooth out

the short-term fluctuations in $\Phi(t)$ and to reveal the long time asymptotic behavior. At long times,

a steady state is reached by the system, corresponding to a value of $\Phi \simeq 0$ and a viscosity which has decreased to a constant value. At this state, the fragments in the wax oil mixture have become very small, and the velocity profile within the fluid is nearly linear, with close to zero slip velocity at the upper and lower surfaces.
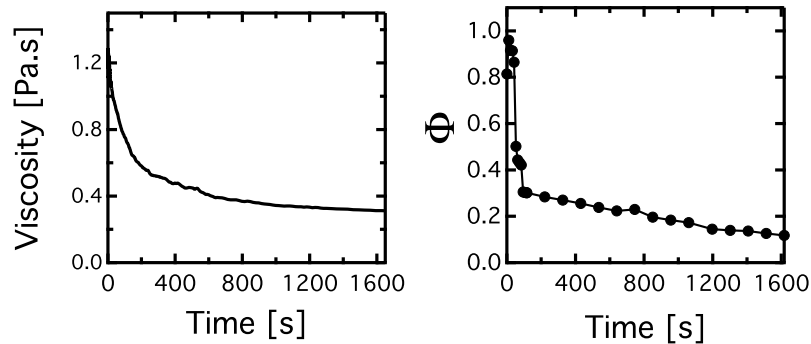

Figure 15: Evolution of viscosity and Φ for a 5% wax in oil system under a steady shear rate of $\dot{\gamma} = 1.5 \mathrm{s}^{-1}$.

In Figure 11, Figure 14 and Figure 15 we have considered evolution of flow profiles for the model wax-oil within a cone plate geometry with a smooth machined aluminum lower surface. We have also demonstrated that the type of surface that the gelled wax/oil is in contact with can have a considerable effect on the behavior of the flow profile (Figure 9). To further explore the role of roughness two experiments were conducted in which a steady shear rate ($\dot{\gamma} = 0.1 s^{-1}$) was imposed on a gelled wax-oil system beneficiated and cooled to 27°C ($T/T_{wa} = 0.993$). For the first experiment, the wax-oil gel was sheared between a smooth upper and lower geometry (as in Figure 11). For the second experiment, the sample was sheared between a roughened lower geometry (root mean square roughness $R_q = 30\mu\mathrm{m}$) and the smooth upper geometry (this configuration is identical to the experiment with the roughened lower surface shown in Figure 10). The bulk rheological data from these experiments is shown in Figure 16. In both instances, the stress within the material reaches a maximum value and then decreases gradually over time. The peak stress for the wax-oil gel in contact with the roughened lower geometry, $\sigma_{\mathrm{max,r}} = 0.89$ Pa is significantly larger than the peak stress for the wax-oil gel in contact with the smooth lower geometry, $\sigma_{\mathrm{max,s}} = 0.41$ Pa. Furthermore the stress within the wax-oil gel is always lower when the sample is in contact with the

29

smooth geometry. This behavior is consistent with the data presented in Figure 10 and Figure 8. At the end of each test the stress in both experiments is still decreasing and has not yet reached a steady state. From the rheological measurements shown in Figure 9 at high stress ($\sigma \gg \sigma_y$), it is expected that the two steady state stress values should ultimately approach the same value at long times, coinciding with a value of $\Phi = 0$ where the structure of the material has broken down completely.
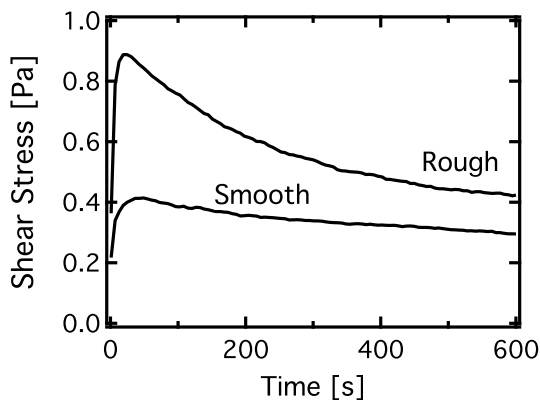

Figure 16: Comparison of stress vs time for a 5% wax-oil system at 27°C ($T/T_{wa} = 0.993$) undergoing steady shear of $\dot{\gamma} = 0.1\text{s}^{-1}$ with a roughened lower surface($R_q = 30\mu$m) and with a smooth lower ($R_q = 0.6\mu$m) surface.

The evolution of local velocity fields for both experiments are represented in the space time plots shown in Figure 17 together with the temporal evolution of the erosion parameter $\Phi(t)$. These space time plots show the same characteristic three-stage behavior documented at the higher shear rate presented in Figure 11. There is an initial stage where the material is strained uniformly (linear growth in the stress and the velocity profile) followed by a period during which the material flows in a plug-like manner. The third stage is characterized by fluctuating velocity profiles that are intermediate between perfectly linear shearing profiles and plug like slip profiles. This stage corresponds to progressive break down of the gelled fragments. Despite their qualitative similarity, there is an important distinction between the two cases shown in Figure 17. When the sample is in contact with the roughened bottom surface, slip along this surface is inhibited: as a result, the bulk of the fluid moves with a velocity V_p close to zero, and the deformation in the material is primarily a result of bulk deformation coupled with fluctuating slip on the top surface. The inhibition of slip

at the bottom surface continues for all times as can be discerned from the lower space time plot in Figure 17 (c).
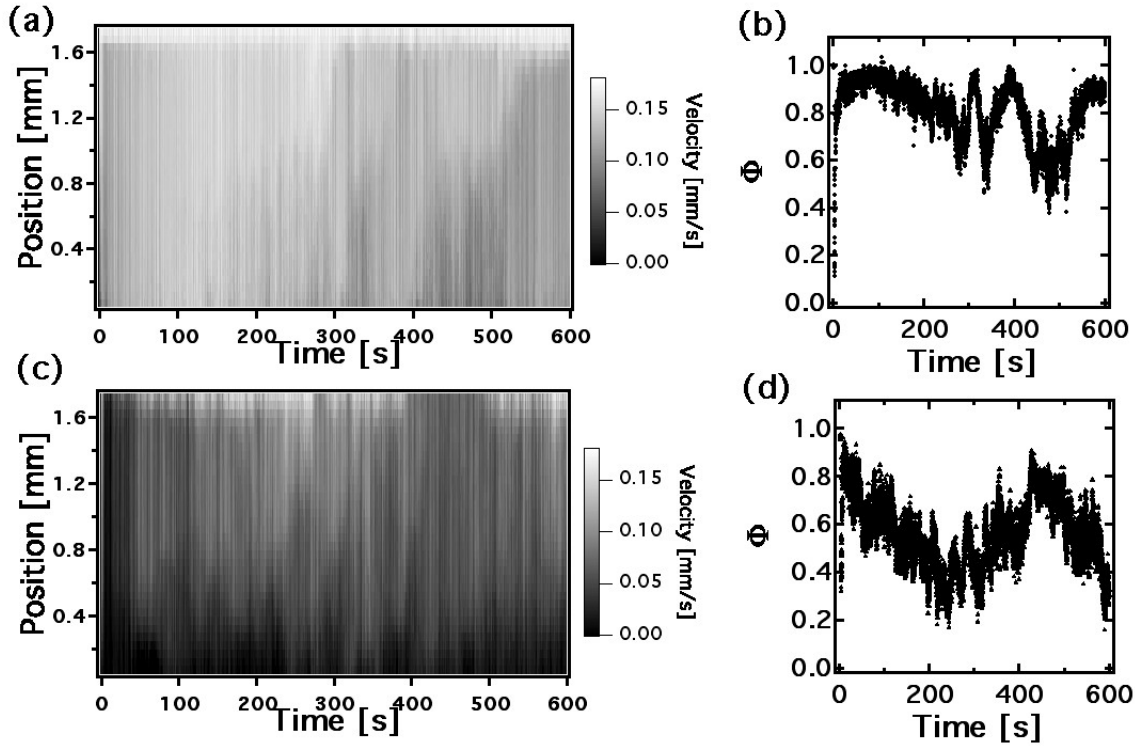

Figure 17: Local velocity field in the form of space-time plots for the 5% wax-oil system undergoing a shear rate of $0.1 \mathrm{s}^{-1}$ at 27°C ($T/T_{wa} = 0.993$) in contact with (a) a smooth lower surface ($R_q = 0.6\mu$m) and in contact with (b) a rough lower surface ($R_q = 30\mu$m). Evolution of Φ given on right hand side of plots ((b) for the smooth lower surface and (d) for the rough lower surface).

The long term fluctuations in the space time plots and the slow decay in the measured shear stress (Figure 16) are reflected in the evolution of the dimensionless erosion parameter $\Phi(t)$ (Figure 17 (b) and (d)). For both experiments, the value of Φ initially increases to a value very close to unity (indicating perfect plug like flow in both cases just after the stress maxima shown in Figure 16). Over the rest of the 10 minute period, Φ decreases in a time-fluctuating manner. This fluctuating behavior of Φ is due to the localized nature of the Rheo-PIV measurements. As mentioned previously flow is observed within an imaging window that is small compared to the total size of the sample. At any given instant in time the Rheo-PIV system observes the local (as opposed to bulk) flow behavior of the sample. For this reason, it is instructive to consider the time averaged value of Φ for each experiment. These values are reported in Table 3 in conjunction with

31

the mean energy dissipation rate per unit volume for each experiment which is defined as

$$\langle \dot{E} \rangle = \frac{1}{t} \int_0^t \dot{E} dt' = \frac{1}{t} \int_0^t \sigma(t) \dot{\gamma} dt' \, , \tag{9}$$

where t is the total time of the experiment.

Table 3: Time averaged values of Φ and volumetric energy dissipation rate $\dot{E}$ for experiments at a steady shear rate of $0.1\mathrm{s}^{-1}$ and $0.3\mathrm{s}^{-1}$ and for samples in contact with smooth ($R_q = 0.6\mu\mathrm{m}$) or rough ($R_q = 30\mu\mathrm{m}$) plates

Experiment		$\langle \Phi \rangle$	$\langle \dot{E} \rangle$ [J/m^{3}s]
$\dot{\gamma} = 0.1\mathrm{s}^{-1}$	smooth	0.81	0.034
$\dot{\gamma} = 0.1\mathrm{s}^{-1}$	rough	0.56	0.058
$\dot{\gamma} = 0.3\mathrm{s}^{-1}$	smooth	0.58	0.14
$\dot{\gamma} = 0.3\mathrm{s}^{-1}$	rough	0.53	0.16

As Table 3 shows, for the same shear rate, the average value of Φ is lower when the material is in contact with the roughened geometry. In addition to this, an increase in the imposed shear rate results in a lower average value of Φ. The roles that the imposed shear rate and surface roughness have on the value of the erosion parameter can be understood by considering the energy dissipated into the material. It is clear from Table 3 that for the higher shear rate experiments ($\dot{\gamma} = 0.3\mathrm{s}^{-1}$) there is a higher rate of energy dissipation into the sample. The higher volumetric rate of energy dissipation results in a lower average value of Φ, since the increased energy dissipated into the system results in more fracturing and erosion of the solid gelled fragments. Using rougher surfaces also results in a larger rate of energy dissipation (at a particular shear rate), so the value of Φ drops faster when the sample is sheared between rough surfaces. This is consistent with the bulk rheological data shown in Figure 8 and Figure 9, which show that smooth shearing surfaces allow slip, which in turn enables the material to flow at lower stresses for a given shear rate and therefore dissipate less energy.

Conclusion

We have developed a Rheo-PIV system that enables simultaneous measurements of bulk averaged material properties (such as stress and strain) and local velocity fields in complex fluids such as waxy crude oils. The measurements of the local velocity and deformation fields can be used to probe local evolution in the microstructural deformation and slip of the sample while under an imposed stress or strain. The model wax-oil systems that have been studied in the present work exhibit a temperature- and composition-dependent rheology similar to real waxy crude oil. When the mixture is cooled below the wax appearance temperature T_{wa} using a careful beneficiation procedure, a percolated network of wax crystallites form that cause the fluid to exhibit a yield stress, σ_y. At stresses below the yield point $\sigma < \sigma_y$ the material is an elastoplastic gel and for high stresses $\sigma > \sigma_y$ it behaves as a strongly shear thinning liquid. The yielding transition is essentially irreversible - the sample spanning structure formed by the precipitated discotic crystallites is disrupted under a large imposed stress and is unable to reform without a subsequent thermal beneficiation and cooling step.

The characteristics of the yielding transition in the wax-oil gel were shown to depend on the nature of the solid surface it is placed in contact with. Smooth surfaces with a lower root mean square roughness R_q promote interfacial slip and this can result in measurements of higher apparent shear rates and a lower apparent viscosity at the same imposed stress. The rheoPIV system can also be used to study the erosion in the local microstructure for a gelled system under controlled deformation rate conditions. When a steady shear rate is imposed the wax-oil gel is initially strained to a critical yield strain and reaches a maximum stress; beyond this point the gel undergoes fluctuating periods of wall slip and structural erosion which results in initially large gelled fragments breaking down into progressively smaller fragments. The rate of erosion can be changed by modifying the characteristics of the bounding surface. Roughened surfaces lead to increased energy dissipation rates, which assist in a more rapid erosion of the gel structure. The combination of time-resolved rheometry and PIV analysis provides new insight into the complex yielding mechanisms experienced by the percolated crystallite structures formed in waxy crude oils, and may ultimately have

an impact on pipeline restart strategies or systematic design and selection of pipe wall surface finishes.

Acknowledgement

References

(1) Speight, J. G. *The Chemistry and Technology of Petroleum*, 4th ed.; CRC Press, 2007.

(2) Wardhaugh, L. T.; Boger, D. V. *AIChE Journal* **1991**, *37*, 871–885.

(3) Venkatesan, R.; Ostlund, J. A.; Chawla, H.; Wattana, P.; Nyden, M.; Fogler, H. S. *Energy and Fuels* **2003**, *17*, 1630–1640.

(4) Winter, H. The critical gel - The universal material state between liquid and solid. *Structure and Dynamics of Polymer and Colloidal Systems*, PO Box 17, 3300 AA Dordrecht Netherlands, 2002; pp 439–470, Conference of the NATO-Advanced-Study-Institute on Structure and Dynamics of Polymer and Colloidal Systems, Les Houches, France, Sep 14-24, 1999.

(5) Winter, H.; Mours, M. *Advances in Polymer Science* **1997**, *134*, 165–234.

(6) Rønningsen, H. P. *Journal of Petroleum Science and Engineering* **1992**, *7*, 177–213.

(7) Kanè, M.; Djabourov, M.; Volle, J.-L.; Lechaire, J.-P.; Frebourg, G. *Fuel* **2002**, *82*, 127–135.

(8) Kanè, M.; Djabourov, M.; Volle, J. *Fuel* **2004**, *83*, 1591–1605, Symposium on Fundamental Mechanisms of Biomass Pyrolysis and Oxidation, Richmond, VA, Oct 28-30, 2002.

(9) Gao, P.; Zhang, J.; Ma, G. *Journal of Physics - Condensed Matter* **2006**, *18*, 11487–11506.

(10) Chin, W. C. *Offshore* **2000**, *60*, 92.

(11) Joshi, N. B.; Muhammad, M.; J., C.; McFadden, J. Flow Assurance: A challenging path to well completions and productivity. *Offshore Technology Conference, 5 May-8 May 2003, Houston, Texas*, 2003.

(12) Hammami, A.; Ratulowski, J. Precipitation and Deposition of Asphaltenes in Production Systems: A Flow Assurance Overview. *Asphaltenes, Heavy Oils, and Petroleomics*, 2007; pp 617–660.

(13) Visintin, R. F. G.; Lapasin, R.; Vignati, E.; D'Antona, P.; Lockhart, T. P. *Langmuir* **2005**, *21*, 6240–6249.

(14) Visintin, R. F. G.; Lockhart, T. P.; Lapasin, R.; D'Antona, P. *Journal of Non-Newtonian Fluid Mechanics* **2008**, *149*, 34–39.

(15) Venkatesan, R.; Nagarajan, N.; Paso, K.; Yi, Y.; Sastry, A.; Fogler, H. *Chemical Engineering Science* **2005**, *60*, 3587–3598.

(16) Russell, R.; Chapman, E. *Journal of the Institute of Petroleum* **1971**, *57*, 117.

(17) Cawkell, M.; Charles, M. *Journal of Pipelines* **1989**, *7*, 251–256.

(18) Pedersen, K. S.; Rønningsen, H. P. *Energy & Fuels* **2000**, *14*, 43–51.

(19) Gibaud, T.; Barentin, C.; Manneville, S. *Phys. Rev. Lett.* **2008**, *101*, 258302.

(20) Gibaud, T.; Barentin, C.; Taberlet, N.; Manneville, S. *Soft Matter* **2009**, *5*, 3026–3037.

(21) Coussot, P.; Raynaud, J. S.; Bertrand, F.; Moucheront, P.; Guilbaud, J. P.; Huynh, H. T.; Jarny, S.; Lesueur, D. *Phys. Rev. Lett.* **2002**, *88*, 218301.

(22) Coussot, P.; Nguyen, Q. D.; Huynh, H. T.; Bonn, D. *Journal of Rheology* **2002**, *46*, 573–589.

(23) Coussot, P.; Tocquer, L.; Lanos, C.; Ovarlez, G. *Journal of Non-Newtonian Fluid Mechanics* **2009**, *158*, 85–90.

(24) Chang, C.; Nguyen, O.; Ronningsen, H. *Journal of Non-Newtonian Fluid Mechanics* **1999**, *87*, 127–154.

(25) Perkins, T. K.; Turner, J. B. *Journal of Petroleum Technology* **1971**, *23*, 301–308.

(26) Lee, H. S.; Singh, P.; Thomason, W. H.; Fogler, H. S. *Energy and Fuels* **2008**, *22*, 480–487.

(27) Singh, P.; Venkatesan, R.; Fogler, H. S.; Nagarajan, N. *AIChE Journal* **2000**, *46*, 1059–1074.

(28) Singh, P.; Venkatesan, R.; Fogler, H. S.; Nagarajan, N. *AIChE Journal* **2001**, *47*, 6–18.

(29) Ghanaei, E.; Mowla, D. *Energy & Fuels* **2010**, *24*, 1762–1770.

(30) Bird, R. B.; Armstrong, R. C.; Hassager, O. *Dynamics of Polymeric Liquids Vol. 1*, 2nd ed.; John Wiley and Sons, 1987.

(31) Larson, R. G. *The Structure and Rheology of Complex Fluids*, Ninth ed.; Oxford University Press, 1999.

(32) Angell, C. A. *Science* **1995**, *267*, 1924–1935.

(33) Padgett, F. W.; Hefley, D. G.; Henriksen, A. *Industrial and Engineering Chemistry* **1926**, *18*, 832–835.

(34) Tapadia, P.; Ravindranath, S.; Wang, S. Q. *Phys. Rev. Lett.* **2006**, *96*, 196001.

(35) Tapadia, P.; Wang, S. Q. *Phys. Rev. Lett.* **2006**, *96*, 016001.

(36) Meeker, S. P.; Bonnecaze, R. T.; Cloitre, M. *Journal of Rheology* **2004**, *48*, 1295–1320.

(37) Meeker, S. P.; Bonnecaze, R. T.; Cloitre, M. *Phys. Rev. Lett.* **2004**, *92*, 198302.

(38) Møller, P.; Fall, A.; Chikkadi, V.; Derks, D.; Bonn, D. *Phil. Trans. R. Soc. A* **2009**, *367*, 5139–5155.

(39) Møller, P. C. F.; Fall, A.; Bonn, D. *Europhysics Letters* **2009**, *87*, 38004.

(40) Chang, C.; Boger, D. V. *Industrial and Engineering Chemistry* **1998**, *37*, 1551–1559.

(41) Møller, P.; Mewis, J.; Bonn, D. *Soft Matter* **2006**, *2*, 274–283.

(42) Barnes, H. A. *Journal of Non-Newtonian Fluid Mechanics* **1995**, *56*, 221–251.

(43) Møller, P. C. F.; Rodts, S.; Michels, M. A. J.; Bonn, D. *Phys. Rev. E* **2008**, *77*, 041507.

(44) Divoux, T.; Tamarii, D.; Barentin, C.; Manneville, S. *Phys. Rev. Lett.* **2010**, *104*, 208301.

(45) Goyon, J.; Colin, A.; Ovarlez, G.; Ajdari, A.; Bocquet, L. *Nature* **2008**, *454*, 84–87.

(46) Bertola, V.; Bertrand, F.; Tabuteau, H.; Bonn, D.; Coussot, P. *Journal of Rheology* **2003**, *47*, 1211–1226.

(47) Lettinga, M. P.; Manneville, S. *Phys. Rev. Lett.* **2009**, *103*, 248302.

(48) Bécu, L.; Manneville, S.; Colin, A. *Phys. Rev. Lett.* **2004**, *93*, 018301.

(49) Yoshimura, A.; Prudhomme, R. K. *Journal of Rheology* **1988**, *32*, 53–67.

(50) Eisenmann, C.; Kim, C.; Mattsson, J.; Weitz, D. A. *Phys. Rev. Lett.* **2010**, *104*, 035502.

(51) Liu, A. J.; Nagel, S. R. *Nature* **1998**, *396*, 21–22.